COMPRESSED SENSING MRI USING TOTAL VARIATION REGULARIZATION WITH K-SPACE DECOMPOSITION

*Liyan Sun, Yue Huang, Congbo Cai, Xinghao Ding**

School of Information Science and Engineering, Xiamen University, Xiamen, China

ABSTRACT

Compressed sensing theory facilitates the fast magnetic resonance imaging by reducing the required number of measurements for reconstruction. Conventional compressed sensing magnetic resonance imaging(CSMRI) method utilize the partial k-space measurements as a whole without considering their intrinsic property. Some recent researches have shown the advantage of dealing the high and low frequency image content separately. Based on this, we propose a novel CSMRI algorithm based on total variation regularization with k-space decomposition. First we decompose k-space into high frequency band and low frequency band, then we reconstruct the corresponding high and low MR images which will be used for integration later. All the steps can be unified into a objective function. We will show that the proposed objective function can be split into several subproblems to solve iteratively using ADMM technique. The experimental results show that the proposed method outperforms the conventional CSMRI method. Besides, the proposed method can be extended to other image processing applications as well.

Index Terms— Magnetic Resonance Imaging, Compressed Sensing, ADMM, K-space Decomposition, Total Variation

1. INTRODUCTION

Although magnetic resonance imaging bas been prove successful as a promising medical imaging technique, its main drawback is the slow imaging speed. The compressed sensing (CS) theory [1, 2] can be introduced to help reduce the number of required k-space measurements, thus shortening the imaging time consumption [3]. According to CS theory, the MR image can be represented sparsely in transform domains. Different sparse domains are proposed in the past researches such as finite difference domain (total variation) [3, 4, 5], regular 2D wavelet domain [3, 6], tight frames domain (contourlet [7],curvelet [8]) and adaptive dictionary bases (DLMRI [9], TLMRI [10], BPTV [11]). Generally, the adaptive bases outperform the nonadaptive bases because of their better representation ability. Structural sparse prior such as group sparsity [12] and nonlocal property of MR images [13, 14] are also utilized to promote the reconstruction. Besides the work mentioned above, the deep learning technique like convolutional neural network (CNN) is also introduced to directly learn the nonlinear mapping [15]. The MR imaging can be accelerated significantly using the CNN architecture.

There are also some work focusing on the exploitation of the different bands of k-space data. In [16], the low frequency region of k-space is first reconstructed, then the original low frequency region is replaced by the reconstructed low frequency data. The fused renewed k-space measurement is then used for final reconstruction. The method outperforms the conventional CSMRI method, but its main shortcoming is the reconstruction error in low frequency region may be propagated to later reconstruction. In another work called CoCCo [17], the MR image is first convolved with a series of directional filters to obtain the corresponding features as constraints, then these constraint images are used for later fusion to yield the reconstruction. Although the work achieves superior performance than regular CSMRI methods, it's intuitive and heuristic without a unifying objective function, which may obstruct the further development of the k-space decomposition idea.

All the work above inspire us to decompose the k-space measurements into different frequency bands, and treat them separately during the reconstruction. Based on this, we propose a novel CSMRI method based on total variation regularization with k-space decomposition. The contributions of the paper can be concluded as follow:

- We decompose the k-space measurement to separate it into high frequency regions and low frequency regions. In this way, more accurate information can be provided for reconstruction. Different prior information of high/low frequency region can be better exploited.

- We unify the decomposition, reconstruction and integration stages in a unified objective function and intro-

*Corresponding author: dxh@xmu.edu.cn. The work is supported in part by National Natural Science Foundation of China under Grants 61571382, 81671766, 61571005, 81671674, U1605252, 61671309 and 81301278, Guangdong Natural Science Foundation under Grant 2015A030313007, Fundamental Research Funds for the Central Universities under Grant 20720160075, 20720150169, CCF-Tencent research fund, Natural Science Foundation of Fujian Province of China (No.2017J01126), and the Science and Technology funds from the Fujian Provincial Administration of Surveying, Mapping, and Geoinformation.

duce ADMM [18] technique to split the objective function into several subproblems easier to solve iteratively.

2. PROBLEM FOURMULATION

As we can see in Fig. 1, the image corresponding to the high frequency k-space data is much more sparse containing fine structural information like contours and curves, while the MR image corresponding to the low frequency k-space data makes up the majority of the energy and exhibit the rough outlook of the whole image. It's shown that different k-space regions exhibit different property, so it's reasonable to decompose k-space into high and low regions and reconstruct them separately before integration. It will bring the benefits that prior is exploited more finely and high frequency information is recovered better. We formulate the whole objective function as

$$\begin{aligned} x = \arg\min_{x} & \tfrac{\lambda}{2} \left\| F_u x - y \right\|_2^2 + \tfrac{\lambda_h}{2} \left\| F_u x_h - y_h \right\|_2^2 \\ & + \tfrac{\lambda_l}{2} \left\| F_u x_l - y_l \right\|_2^2 + \mu_h TV\left(x_h\right) + \mu_l TV\left(x_l\right) \\ s.t. \quad & H_h x = x_h, H_l x = x_l \end{aligned} \tag{1}$$

Where $F_u \in \mathbb{C}^{M \times N} (M < N)$ denotes the undersampling Fourier matrix. If $M = N$ holds, the F_u will be turned into Fourier transform matrix F. $x \in \mathbb{C}^{N \times 1}$ is the vectorized MR image to be reconstructed and $y \in \mathbb{C}^{M \times 1}$ denotes the undersampled k-space measurements. x_h and x_l is the high and low frequency MR image to be reconstructed respectively. y_l and y_h is the corresponding decomposed k-space measurements. λ is the regularization parameter, while λ_h and λ_l is the regularization parameters for high/low frequency reconstruction. We adopt total variation as the reconstruction method for high and low frequency data because of its efficiency and popularity. Note that different CSMRI methods can be applied during the reconstruction. H_l and H_h denote the low and high 2D filter in block Toeplitz matrix form corresponding to the 2D spatial filter for later convenient mathematical derivation. The constraint terms show that x_h and x_l is obtained via the convolution between the filters and the image to be reconstructed.

3. OPTIMIZATION

We adopt the alternating direction multiplier method (ADMM) to tackle the objective function. ADMM method is an efficient convex optimization method. Using ADMM technique, we split the objective function into three subproblems,

$$\begin{aligned} (1) \quad & x_h^{t+1} = \arg\min_{x_h} \tfrac{\lambda_h}{2} \left\| F_u x_h^t - y_h \right\|_2^2 \\ & \quad + \tfrac{\gamma_h}{2} \left\| H_h x^t - x_h^t + E_h^t \right\|_2^2 + \mu_h \left\| D x_h^t \right\|_1 \\ & x_l^{t+1} = \arg\min_{x_l} \tfrac{\lambda_l}{2} \left\| F_u x_l^t - y_l \right\|_2^2 \\ & \quad + \tfrac{\gamma_l}{2} \left\| H_l x^t - x_l^t + E_l^t \right\|_2^2 + \mu_l \left\| D x_l^t \right\|_1 \\ (2) \quad & x^{t+1} = \arg\min \tfrac{\lambda}{2} \left\| F_u x^t - y \right\|_2^2 \\ & \quad + \tfrac{\gamma_l}{2} \left\| H_l x^t - x_l^t + E_l^t \right\|_2^2 \\ & \quad + \tfrac{\gamma_h}{2} \left\| H_h x^t - x_h^t + E_h^t \right\|_2^2 \\ (3) \quad & E_h^{t+1} = H_h x^{t+1} - x_h^{t+1} + E_h^t \\ & E_l^{t+1} = H_l x^{t+1} - x_l^{t+1} + E_l^t \end{aligned} \tag{2}$$

Where D is the finite difference matrix defined in total variation method. μ_l, μ_h ,γ_l, γ_h and λ_l, λ_h are the related regularization parameters set manually.

We iteratively optimize the three problems and obtain the updated x_l, x_h and x, the optimization will finally converge to the optimal as the iteration goes. The iteration will stop when the distance between consecutive images x^t and x^{t+1} is smaller than a threshold η. E_h and E_l are the ADMM multipliers, which are updated at the end of each iteration.

3.1. Acquiring high and low frequency measurements

As we can see, we need to acquire the high and low frequency k-space measurements for high and low frequency MR image reconstruction. We decompose original k-space measurements into high frequency region and low frequency region using 2D Gaussian filter. We denote the high and low 2D Gaussian filter as h_h and h_l and the 2D form of x as X. The corresponding high and low frequency MR images are

$$X_h = h_h * X, \quad X_l = h_l * X \tag{3}$$

It is known that the 2D convolution in spatial domain is equivalent to 2D hadamard multiplication in frequency domain, so we reformulate Eq. 3 as

$$\hat{X}_h = \hat{H}_h \cdot \hat{X}, \quad \hat{X}_l = \hat{H}_l \cdot \hat{X} \tag{4}$$

Where all the uppercase variables with hat in Eq. 4 are the frequency form of the corresponding lowercase variables in Eq. 3. Note the size of h_l and h_h are of much smaller size of X, so we pad the h_h and h_l to the same size as reconstructed images before transformed into frequency domain. The frequency responses of h_h and h_l satisfy the complementary property: $\hat{H}_l$ + $\hat{H}_h$ = **1**. Furthermore, the original k-space measurements in 2D form is

$$Y = M \cdot \hat{X} \tag{5}$$

Where M is the undersampling pattern. According to Eq. 3 and Eq. 4, we yield

$$Y_h = M \cdot \hat{X}_h = M \cdot \hat{H}_h \cdot \hat{X} = Y \cdot \hat{H}_h \tag{6}$$

It shows that the high and low k-space measurements can be obtained by the hadamard product of the original 2D k-space measurements and the frequency responses of the Gaussian filters. We can obtain y_l and y_h after vectorization.

3.2. High and low MR image reconstruction

Since the high frequency MR reconstruction is in the same form of low frequency MR reconstruction, we take high frequency case for example. The high frequency MR imaging reconstruction can be formulated as

$$\begin{aligned} x_h^{t+1} = \arg\min_{x_h} & \tfrac{\lambda_h}{2} \left\| F_u x_h^t - y_h \right\|_2^2 \\ & + \tfrac{\gamma_h}{2} \left\| H_h x^t - x_h^t + E_h^t \right\|_2^2 + \mu_h \left\| D x_h^t \right\|_1 \end{aligned} \tag{7}$$

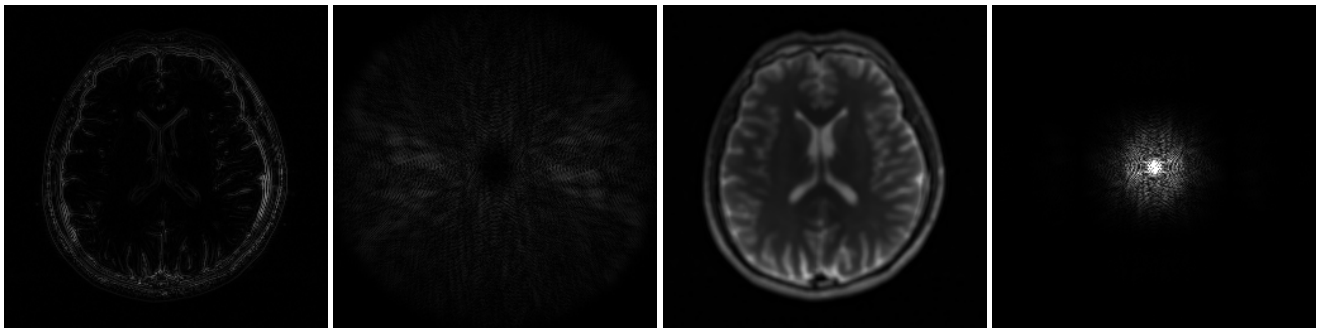

(a) high frequency MR image (b) high frequency data (c) low frequency MR image (d) low frequency data

Fig. 1. The high/low frequency MR images. The right side shows the corresponding k-space data.

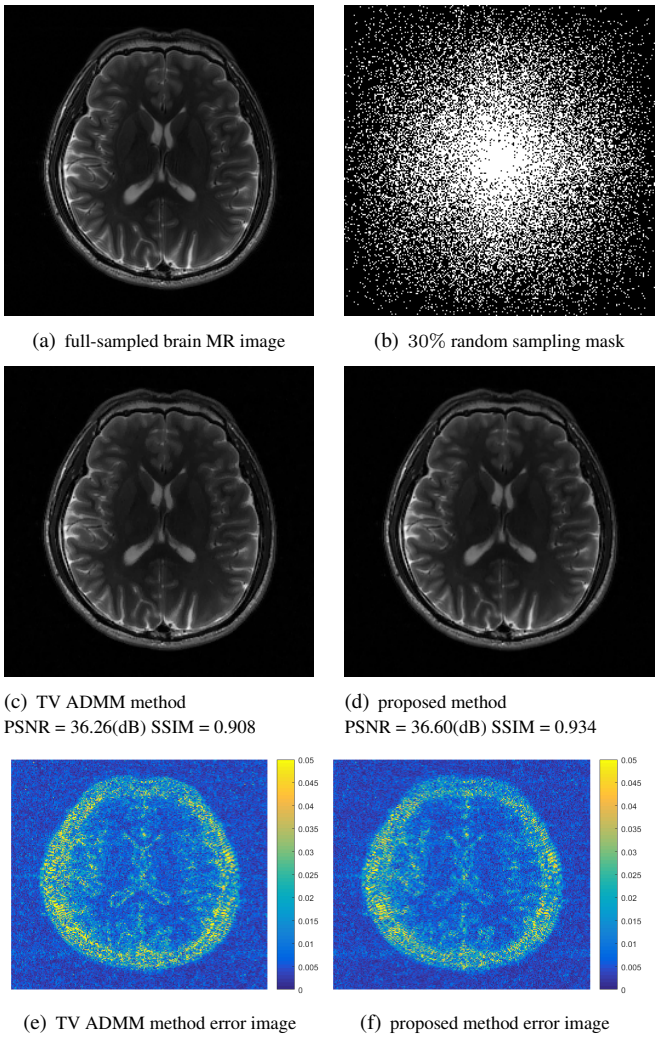

(a) full-sampled brain MR image (b) 30% random sampling mask

(c) TV ADMM method
PSNR = 36.26(dB) SSIM = 0.908

(d) proposed method
PSNR = 36.60(dB) SSIM = 0.934

(e) TV ADMM method error image (f) proposed method error image

Fig. 2. The experimental results of the 10^{th} slice of the T2-weighted complex-valued brain image. We show the subjective reconstruction results on 30% random under-sampling mask.

The objective function is typically an $\ell_2 - \ell_2 - \ell_1$ problem, which also can be solved using ADMM method. We introduce the auxiliary variable u_h for optimization.

$$x_h^{t+1} = \arg\min_{x_h} \frac{\lambda_h}{2} \|F_u x_h^t - y_h\|_2^2 + \frac{\gamma_h}{2} \|H_h x^t - x_h^t + E_h^t\| + \mu_h \|u_h\|_1 + \frac{\beta_h}{2} \|Dx_h^t - u_h + O\|_2^2 \tag{8}$$

Similarly, we can split the objective function Eq. 8 into three subproblems,

$$\begin{aligned} &(1)\ u_h' = \arg\min_{u_h} \tfrac{\beta_h}{2} \|Dx_h^t - u_h + O\|_2^2 + \mu_h \|u_h\|_1 \\ &(2)\ x_h^{t\,\prime} = \arg\min_{x_h^t} \tfrac{\lambda_h}{2} \|F_u x_h^t - y_h\|_2^2 + \\ &\qquad \tfrac{\gamma_h}{2} \|H_h x^t - x_h^t + E_h^t\|_2^2 + \tfrac{\beta_h}{2} \|Dx_h^t - u_h + O\|_2^2 \\ &(3)\ O' = Dx_h^t - u_h + O \end{aligned} \tag{9}$$

We first do soft-thresholding algorithm to get the auxiliary variable u_h, then we solve a least square problem to get the estimation of x_h [11], followed by the update of the Lagrangian multiplier O . The three subproblems are solved iteratively until the distance between the consecutive reconstruction result is smaller than a threshold η_{in}.

$$\begin{aligned} &(1)\ u_h{}' = SoftThres\left(Dx_h^t + O, \tfrac{2\mu_h}{\beta_h}\right) \\ &(2)\ x_h^{t\,\prime} = F^H \tfrac{\lambda_h F F_u^H y_h + \beta_h F D^H \left(u^t - O\right) + \gamma_h F \left(H_h x^t + E_h^t\right)}{\lambda_h F F_u^H F_u F^H + \beta_h F D^H D F^H + \gamma_h} \\ &(3)\ O' = Dx_h^t - u^t + O \end{aligned} \tag{10}$$

3.3. High and low MR image integration

After we get both x_l and x_h, we can integrate them using least square method to obtain the reconstructed MR image x^{t+1} in this iteration.

$$x^{t+1} = F^H \frac{\lambda F F_u^H y + \gamma_l F H_l^H \left(x_l^t - E_l^t\right) + \gamma_h F H_h^H \left(x_h^t - E_h^t\right)}{\lambda F F_u^H F_u F^H + \gamma_l F H_l^H H_l F^H + \gamma_h F H_h^H H_h F^H} \tag{11}$$

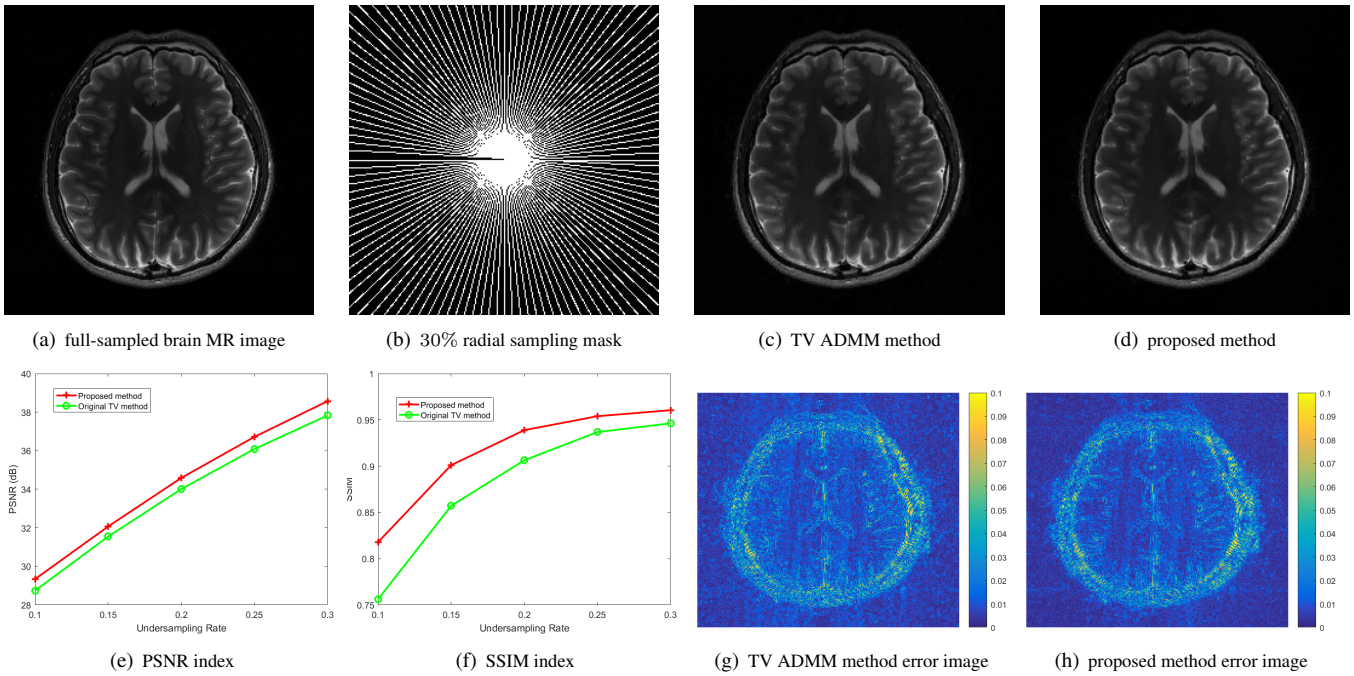

(a) full-sampled brain MR image (b) 30% radial sampling mask (c) TV ADMM method (d) proposed method

(e) PSNR index (f) SSIM index (g) TV ADMM method error image (h) proposed method error image

Fig. 3. The experimental results of the 27^{th} slice of the T2-weighted complex-valued brain image. We show the subjective reconstruction results on 30% radial under-sampling mask. We also plot the objective evaluation indexes.

3.4. Multiplier updating

At the end of ADMM iteration, we update the multipliers according to the third subproblems. The multipliers updating process can be viewed as denoising process according to ADMM theory. The proposed method is comprised of an inner ADMM optimization loop and a outer ADMM optimization loop. Only after the converge of each inner loop, the outer loop goes on. This process continue until the outer loop stop criteria is satisfied.

4. EXPERIMENTS

To test the effectiveness and efficiency of the proposed algorithm, we conduct the experiments on complex-valued brain data. We set parameters the same for all the experiment data to prove the stability of the proposed algorithm: $\lambda = \lambda_l = \lambda_h = 1e6$, $\gamma_l = \gamma_h = 1e2$, $\eta = 5e-3$, $\eta_{in} = 1e-3$, $\mu_l = \mu_h = 1$, $\beta_h = \beta_l = 800$. The size of Gaussian filter is 5×5 and the standard deviation is set 0.6. We conduct the experiments on the brain image series acquired from a healthy volunteer by a 3-T Siemens Trio Tim MRI scanner using the T2-weighted turbo spin echo sequence (TR/TE = $6100/99ms$, $220 \times 220mm^2$ field of view, 3-mm slice thickness) [14]. We choose the 10^{th} slice and 27^{th} as tested images. Besides, we compare the proposed algorithm with regular TV based CSMRI method. The ADMM technique is also adopted for the optimization with all parameters set optimal. We adopt peak signal noise ratio (PSNR) and structural similarity index measurement (SSIM) as objective evaluation index for their popularity and effectiveness.

We under-sample the 10^{th} slice of the brain data with 2D radial mask at a series sampling ratios. The subjective and objective experimental results are shown in Fig. 3. It's shown that the proposed algorithm outperforms the regular TV based CSMRI at all tested sampling ratios. For the reconstruction results in proposed algorithm, the background noise is better removed and the details are preserved better.

We also conduct the experiment on the 27^{th} slice of the brain data using 30% 2D random mask. As shown in Fig. 2, the structural information is better restored, which may be critical for the diagnosis.

5. CONCLUSION

Conventional CSMRI methods may overlook the intrinsic property of k-space data, and it's reasonable to exploit different region of k-space separately. Based on this analysis, we propose k-space decomposition idea with an unified objective function. The ADMM technique is introduced for optimization. The experimental results show that the proposed method based on total variation regularization outperforms the regular total variation based CSMRI method. The idea can be extended to other image processing applications.

6. REFERENCES

[1] David L Donoho, "Compressed sensing," *IEEE Transactions on information theory*, vol. 52, no. 4, pp. 1289–1306, 2006.

[2] Emmanuel J Candès, Justin Romberg, and Terence Tao, "Robust uncertainty principles: Exact signal reconstruction from highly incomplete frequency information," *IEEE Transactions on information theory*, vol. 52, no. 2, pp. 489–509, 2006.

[3] Michael Lustig, David Donoho, and John M Pauly, "Sparse mri: The application of compressed sensing for rapid mr imaging," *Magnetic resonance in medicine*, vol. 58, no. 6, pp. 1182–1195, 2007.

[4] Leonid I Rudin, Stanley Osher, and Emad Fatemi, "Nonlinear total variation based noise removal algorithms," *Physica D: Nonlinear Phenomena*, vol. 60, no. 1-4, pp. 259–268, 1992.

[5] Antonin Chambolle, "An algorithm for total variation minimization and applications," *Journal of Mathematical imaging and vision*, vol. 20, no. 1, pp. 89–97, 2004.

[6] Stephane G Mallat, "A theory for multiresolution signal decomposition: the wavelet representation," *IEEE transactions on pattern analysis and machine intelligence*, vol. 11, no. 7, pp. 674–693, 1989.

[7] Xiaobo Qu, Weiru Zhang, Di Guo, Congbo Cai, Shuhui Cai, and Zhong Chen, "Iterative thresholding compressed sensing mri based on contourlet transform," *Inverse Problems in Science and Engineering*, vol. 18, no. 6, pp. 737–758, 2010.

[8] Jean-Luc Starck, Emmanuel J Candés, and David L Donoho, "The curvelet transform for image denoising," *IEEE Transactions on image processing*, vol. 11, no. 6, pp. 670–684, 2002.

[9] Saiprasad Ravishankar and Yoram Bresler, "Mr image reconstruction from highly undersampled k-space data by dictionary learning," *IEEE transactions on medical imaging*, vol. 30, no. 5, pp. 1028–1041, 2011.

[10] Saiprasad Ravishankar and Yoram Bresler, "Sparsifying transform learning for compressed sensing mri," in *Biomedical Imaging (ISBI), 2013 IEEE 10th International Symposium on*. IEEE, 2013, pp. 17–20.

[11] Yue Huang, John Paisley, Qin Lin, Xinghao Ding, Xueyang Fu, and Xiao-Ping Zhang, "Bayesian nonparametric dictionary learning for compressed sensing mri," *IEEE Transactions on Image Processing*, vol. 23, no. 12, pp. 5007–5019, 2014.

[12] Chen Chen and Junzhou Huang, "Compressive sensing mri with wavelet tree sparsity," in *Advances in neural information processing systems*, 2012, pp. 1115–1123.

[13] Weisheng Dong, Guangming Shi, Xin Li, Yi Ma, and Feng Huang, "Compressive sensing via nonlocal low-rank regularization," *IEEE Transactions on Image Processing*, vol. 23, no. 8, pp. 3618–3632, 2014.

[14] Xiaobo Qu, Yingkun Hou, Fan Lam, Di Guo, Jianhui Zhong, and Zhong Chen, "Magnetic resonance image reconstruction from undersampled measurements using a patch-based nonlocal operator," *Medical image analysis*, vol. 18, no. 6, pp. 843–856, 2014.

[15] Shanshan Wang, Zhenghang Su, Leslie Ying, Xi Peng, Shun Zhu, Feng Liang, Dagan Feng, and Dong Liang, "Accelerating magnetic resonance imaging via deep learning," in *Biomedical Imaging (ISBI), 2016 IEEE 13th International Symposium on*. IEEE, 2016, pp. 514–517.

[16] Yang Yang, Feng Liu, Wenlong Xu, and Stuart Crozier, "Compressed sensing mri via two-stage reconstruction," *IEEE Transactions on Biomedical Engineering*, vol. 62, no. 1, pp. 110–118, 2015.

[17] Xi Peng and Dong Liang, "Mr image reconstruction with convolutional characteristic constraint (cocco)," *IEEE Signal Processing Letters*, vol. 22, no. 8, pp. 1184–1188, 2015.

[18] Stephen Boyd, Neal Parikh, Eric Chu, Borja Peleato, and Jonathan Eckstein, "Distributed optimization and statistical learning via the alternating direction method of multipliers," *Foundations and Trends® in Machine Learning*, vol. 3, no. 1, pp. 1–122, 2011.